Available online at www.sciencedirect.com

ScienceDirect

IFAC PapersOnLine 59-17 (2025) 19–24

A Multi-physics Model for Phase Change Actuation in Soft Robotics: Towards Untethered Soft Robots

Alexia Le Gall * **Mattia Franchi de' Cavalieri** ** **Matteo Cianchetti** ***

* *Institute of BioRobotics, Scuola Superiore Sant'Anna, Pontedera, 56025 Italy (e-mail: Alexia.LeGall@santannapisa.it).*
** *Institute of BioRobotics, Scuola Superiore Sant'Anna, Pontedera, 56025 Italy (e-mail: mattia.franchidecavalieri@santannapisa.it)*
*** *Institute of BioRobotics, Scuola Superiore Sant'Anna, Pontedera, 56025 Italy (e-mail: matteo.cianchetti@santannapisa.it)*

Abstract: This paper presents a multi-physics model for phase-change-driven actuation in soft robotics, focusing on untethered systems that autonomously generate pressure through liquid evaporation. The model integrates electrothermal, thermo-fluidic, and mechanical domains, coupling Peltier-based heating, vapor generation, and soft material deformation. By operating in a pre-boiling regime, the approach minimises thermal gradients, enhances responsiveness, and reduces energy consumption. The governing equations are integrated into a multiphysics model, providing an innovative tool for designing efficient, safe, and controllable actuators with applications in robotics, biomedical devices, and adaptive materials.

Keywords: Soft robotic actuators; Phase-change actuation; Untethered robotics; Peltier-driven actuation; Multiphysics modelling; Thermofluidic systems; Energy-efficient actuation; Pre-boiling regime;

1. INTRODUCTION

One of the main strengths of soft robotics is its ability to interact safely with different environments. From navigating uneven terrains to handling delicate surfaces, the inherent compliance of soft systems upon contact makes them suitable for a previously unattainable range of applications. This unique property has placed soft robotics as an innovative field that could have a significant impact in the fields of automation, healthcare, and exploration.
Among the various types of actuators in soft robotics, pneumatic-based actuators are one of the most widely adopted solutions. The reasons are multiple: pneumatic systems offer safe operation, high output in strain-to-stress ratios, and excellent efficiency (Huber et al. (1997-10-08)). Additionally, advancements in fabrication methods have allowed for diverse and tailored actuator designs: techniques range from conventional methods like injection moulding, to modern innovations such as 3D printing, enabling the creation of actuators with intricate geometries and varying sizes (Schmitt et al. (2018)).

Pneumatic soft actuators, although they offer numerous advantages, function essentially as transducers converting one type of mechanical power $P_{fluid} = Q \cdot P$ (fluid flow and pressure) into another $P_{mech} = F \cdot v$ (force and velocity). For these systems to operate autonomously, electrical power must first be converted into mechanical power to generate internal pressure in the actuator. Typically, this requires integrating components, such as compressors and valves, in the system; however, these off-the-shelf components often exhibit bulkiness, rigidity and lack compability for seamless integration into soft systems.
A critical research direction in soft robotics is developing untethered systems capable of autonomously generating internal pressure. From the literature, three primary pressure generation approaches have been identified:

- **Fluid displacement**: This approach inflates the chambers using fluid from an external reservoir (Li et al. (2021), Bell et al. (2022)); it is efficient but requires either a pump or auxiliary actuation for the air supply, increasing the complexity of the system and the dependence on additional components.
- **Chemical reactions**: This approach entails either the combination of two reactive components (Wehner et al. (2016)) or the activation of the decomposition of a compound - such as hydrogen peroxide into hydrogen and oxygen - by combustion or electrical input (Wehner et al. (2014), Xu et al. (2021)). Although these methods enable rapid gas generation, they are typically irreversible and difficult to control, adding additional challenges in ensuring consistent and predictable performance.
- **Phase change**: This approach uses the evaporation of a liquid into a gas. A phase change is a thermodynamic process driven by heat transfer. It is often initiated through Joule heating, where electri-

---

⋆ We acknowledge the support of the European Union by the Next Generation EU project ECS00000017 'Ecosis tema dell'Innovazione' Tuscany Health Ecosystem (THE, PNRR, Spoke 9: Robotics and Automation for Health)

10.1016/j.ifacol.2025.10.133

cal energy dissipates as resistive heat, even though alternative heat generation methods have been successfully implemented Han et al. (2019). Initially, the liquid is heated; once the liquid reaches the saturation temperature, vaporisation begins, with both liquid and vapour coexisting in the chamber without further changes in temperature until the liquid fully vaporises. In confined chambers, the vapour exerts uniform pressure on the walls and generates mechanical work by deformation. This mechanism offers a reliable method of actuation; however, it also presents challenges stemming from the complexity involved in developing a multi-physics system. It requires optimising several interdependent parameters to ensure efficient performance.

The efficiency and responsiveness of thermal actuation systems remain a significant challenge, especially in systems where heat transfer is dominated by convection, which often results in prolonged actuation cycles. To overcome these limitations, our model incorporates a Peltier element-based heating system that can both heat up and cool down. This approach optimises thermal control, enabling precise and rapid actuation to address the demands of modern applications (Exley et al. (2023)).

A crucial aspect of this method is the integration of fluid in the system. While porous foams simplify liquid distribution, they tend to deplete quickly, requiring frequent refills (Garrad et al. (2021)). To overcome this, most actuators rely on sealed pouches, which provide durability but demand careful thermal and material engineering. In our model, sealed liquid reservoirs are used to ensure controlled evaporation and reduce system variability.
Liquid selection is another cornerstone of the design. Low-boiling-point fluids such as *3M Novec* fluids (30–80°C), acetone, or ethanol are efficient due to their reduced energy demands for phase change (Garrad et al. (2021)). However, their volatility poses safety risks. Conversely, water, while safer and more accessible, requires significantly more energy due to its higher boiling point. In this study, we leverage the Peltier element's versatile thermal control to explore a balance between efficiency and safety by operating within a pre-boiling regime of a liquid.
Thermal control is paramount for improving both actuation speed and system responsiveness. Excessive heating not only slows the cooling process, often exceeding actuation times by factors of 3 to 10 (Garrad et al. (2019)) but also risks thermal damage. Strategies such as droplet atomization (Lee et al. (2021)) have been proposed to expedite time response, though they often increase system complexity. In contrast, the dual functionality of Peltier elements enables simultaneous heating and cooling, streamlining the system while ensuring precise thermal management (Exley et al. (2023)).

This work proposes the basic equations for harnessing the Peltier effect within a well-defined thermal regime, addressing common limitations of phase-change actuation systems. The goal is to lay the groundwork for developing more efficient and controllable solutions, paving the way for next-generation soft robotic actuators with improved reliability and adaptability across diverse applications.

2. GOVERNING EQUATIONS

2.1 Overview of the model

Our system is modelled as a standalone closed system in an environment with a constant temperature $T_{env} = 25°C$ and atmospheric pressure $P_{env} = 101325[Pa]$. The system consists of a Peltier Element powered by a current source, which heats a reservoir of liquid that is directly connected to a soft chamber shaped like a spherical bubble. A schematic view is proposed in Fig.1a. To simplify the model, we adopt the following assumptions :

- There are no thermic losses from the liquid to the environment except from the soft chamber surface.
- The system is considered quasi-static, transitioning between equilibrium states in discrete time steps Δt.
- The heat generated on the side B of the Peltier element is dissipated instantaneously.
- The environmental temperature and pressure remain constant throughout the simulation.
- The actuator is modelled as an elastic sphere with a thickness d_{shell}.

Those assumptions provide a necessary yet significant simplification of the system, enabling a more tractable analysis. To study this system, we divided its functioning into three phases :

- The Electro-Thermal Phase models the transformation of a current $I[A]$ into a heat flow $Q_A[W]$ transmitted to the liquid.
- The Thermo-Fluidic Phase studies the repartition of $Q_A[W]$ within the system, assimilating it to a thermic circuit as illustrated in Fig.1b. Our primary focus is the evaporation of the liquid, quantified as $m_{vap}[kg]$, which occurs through a mass transfer process illustrated in Fig.1c.
- The fluid-kinetic phase links the increase of pressure $P_G[Pa]$ in the chamber per evaporation to the deformation of the chamber, through the increase of the radius $r[m]$

The overall processes and main variables are depicted in Fig.2.

2.2 Electro-Thermal Phase : The Peltier Device

Peltier devices consist of a series of thermocouples made of different semiconductors, one p-type and the other n-type. Depending on the polarity of the electrical current crossing the elements, electrons are moved, causing either energy generation or consumption. This causes one side of the Peltier module to heat, while the other one cools down. The heat flows $Q_i[W]$ generated at sides A and B can be expressed as the sum of three main contributions:

$$\begin{aligned} &Q_A(t) = Q_{Seebeck,a}(t) - Q_{conduction}(t) + Q_{Joule}(t) \\ &Q_B(t) = -Q_A(t) \end{aligned} \tag{1}$$

With the Seebeck Effect being the direct conversion of the electrical transport and immediate temperature $T[K]$ on side i to the temperature gradient, through the Seebeck coefficient $\alpha[V/K]$:

$$Q_{Seebeck,I}(t) = \alpha \cdot T_i(t) \cdot I(t) \tag{2}$$

The Joule heating caused by the intrinsic resistance $R_p[\Omega]$ of the module to the current $I[A]$

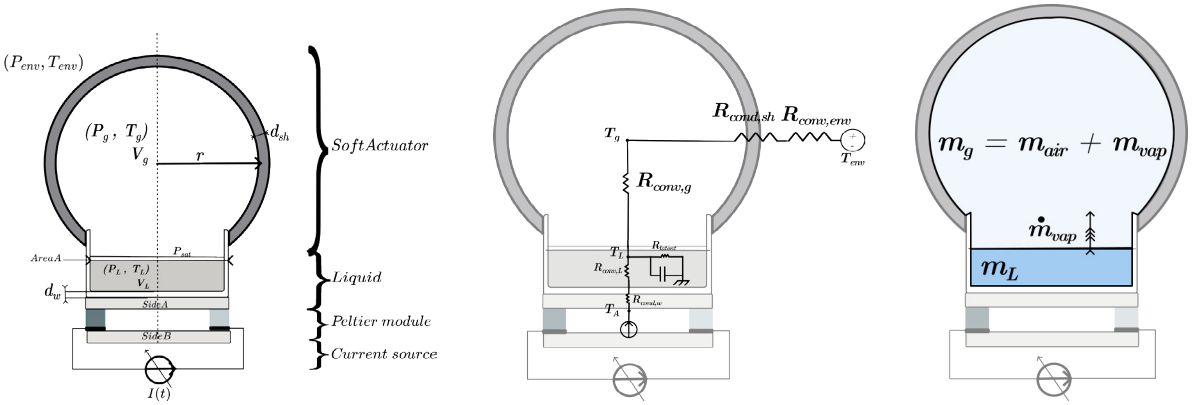

(a) Schematic of the system modelled and main parameters (b) Schematic of the thermic system as modelled (c) Schematic of the fluidic masses exchanged

Fig. 1. Schematic view of the system proposed

$$Q_{Joule}(t) = \frac{1}{2} \cdot R_p \cdot I(t)^2 \tag{3}$$

Due to the thermal gradient, the conduction losses between sides A and B are proportional to $K_p[W/K]$, the thermal conductance of the Peltier module.

$$Q_{conduction}(t) = K_p \cdot (T_A(t) - T_B) \tag{4}$$

From equations (1) - (4) we define Q_A as :

$$Q_A(t) = \frac{R_p}{2} \cdot I(t)^2 + (\alpha \cdot I(t) - K_p) \cdot T_A(t) + K_p \cdot T_B \tag{5}$$

This relationship defines the link between external temperatures, the intensity supplied, and the heat flow generated by the Peltier element.

2.3 Thermo-fluidic Phase

The heat flow Q_A transferred to the liquid drives the evaporation at a rate $\dot{m}_{vap}[kg/s]$, from which we can deduce the increase of vapor for a time step Δt in our system.

Interfaces Because we assume our system to be quasi-static, we can model it as a lumped circuit, analogous to the electrical circuit illustrated in Fig.1b.Convection and conduction are assimilated to resistive processes whereas the Peltier device is modelled as a current source Q_A. Heat is then transferred through a membrane via conduction and through the liquid via convection, therefore :

$$\begin{aligned} Q_A(t) &= \frac{1}{R_{cond,w} + R_{conv,L}} \cdot (T_L(t) - T_A(t)) \\ &= \underbrace{\frac{k_w \cdot A_L \cdot h_L}{h_L \cdot d_w + k_L}}_{\lambda_{wall}} \cdot (T_L(t) - T_A(t)) \end{aligned} \tag{6}$$

We equate the area of contact between the Peltier and the reservoir, as well as the area of the reservoir in contact with the liquid to $A_w[m^2] \approx A_L[m^2]$. The thermal resistance associated with conduction is determined by the wall's material thermal conductivity $k_w[W \cdot m^{-1} \cdot K^{-1}]$,the contact area $A_w[m^2]$, and thickness $d_w[m]$. In contrast, convection is driven by the temperature gradient through the liquid proportionally to the area of contact A_w, and the heat transfer coefficient $h_L[W \cdot K^{-1} \cdot m^{-2}]$. Similarly, heat from the liquid is conveyed through convection and then conduction into the environment as :

$$\begin{aligned} Q_g &= \frac{(T_{env} - T_L(t))}{R_{conv,g} + R_{cond,sh} + R_{conv,env}} \\ &= \lambda_g(t) \cdot (T_{env} - T_L(t)) \end{aligned} \tag{7}$$

With :

$$\lambda_g(t) = \frac{(h_g \cdot A_{sh}(t) \cdot A_L \cdot k_{sh})}{(k_{sh} \cdot A_{sh}(t)) + A_L \cdot (d_{sh} \cdot h_g + k_{sh})} \tag{8}$$

Which can also be expressed as:

$$\begin{aligned} Q_g &= \frac{(T_{env} - T_g(t))}{R_{conv,g} + R_{cond,sh}} \\ &= \lambda_{sh}(t) \cdot (T_{env} - T_g(t)) \\ With : \lambda_{sh}(t) &= \frac{h_g \cdot A_{sh}(t) \cdot k_{sh}}{k_{sh} + d_{sh} \cdot h_g} \end{aligned} \tag{9}$$

Or as a function of T_G and T_L:

$$Q_g(t) = h_G \cdot A_L \cdot (T_G(t) - T_L(t)) \tag{10}$$

In the liquid When the liquid temperature T_L is below the boiling point, the heat flow $Q_{cond,L}$ is conveyed through the liquid then parteyed between being stocked as sensible heat Q_{cap}, or as latent heat Q_{vap} motivating the evaporation, or to escape the liquid through convection Q_g. By summing up the heat flow within the liquid at temperature T_L, we obtain:

$$Q_A(t) = Q_{vap}(t) + Q_{cap}(t) + Q_G(t) \tag{11}$$

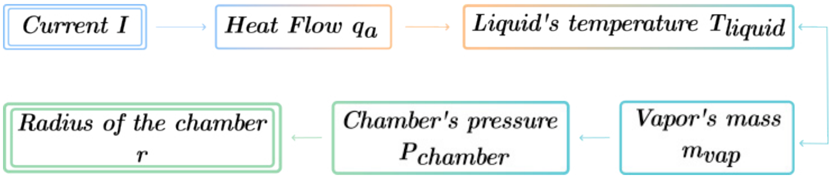

Fig. 2. Bloc-view of the model, highlighting all the time-varying parameters and their interconnections through the four domains.

The portion of the heat flow that is stored in the liquid and contributes to its increase in temperature is modelled as a thermal capacitance. This capacitance represents the ability of the liquid to store heat energy and is a function of its specific heat capacity $c_p[J \cdot kg^{-1} \cdot K^{-1}]$, density, and volume.

$$\begin{aligned} Q_{cap} &= C_L \cdot \frac{dT_L(t)}{dt} \\ &= m_L \cdot c_{p,L} \cdot \frac{dT_L(t)}{dt} \end{aligned} \tag{12}$$

In summary, the heat flow within the liquid at temperature T_L is partitioned into sensible heat, latent heat, and convective losses, with the thermal capacitance modelling the liquid's capacity to store heat energy, thereby influencing its temperature increase.

Nodes and Temperatures Because we are working within a steady-state model, temperatures are assumed to remain constant during each time step Δt. However, to accurately capture the system's behaviour, the temperatures of the circuit—denoted T_L, T_A, and T_G as schematized in Fig.1b, must evolve. We derive those quantities through an Euler-discretization:

$$\frac{dT_L}{dt} = \frac{T_L(t+\Delta t) - T_L(t)}{\Delta t} \tag{13}$$

The increase in the temperature of the liquid T_L as referenced in equations (12) and (11) can be expressed as follows :

$$T_L(t+\Delta t) = (Q_A - Q_{vap} - Q_G) \cdot \frac{\Delta t}{C_L} + T_L(t) \tag{14}$$

When T_A can be defined as a function of T_L and I, it is derived from the equations (5) and (6) :

$$T_A(t) = \frac{\lambda_{wall} \cdot T_L(t) - 0.5 \cdot R_p \cdot I(t)^2 - K_p \cdot T_B}{\lambda_{wall} + \alpha \cdot I(t) - K_p} \tag{15}$$

Finally, T_G can be expressed as a function of T_L deriving the equation (9) and (10) as

$$T_G(t) = \frac{\lambda_{sh} \cdot T_{env} + h_G \cdot A_L \cdot T_L(t)}{\lambda_{sh} + h_G \cdot A_L} \tag{16}$$

Evaporation To calculate T_L, it is essential to first estimate the heat flow repartition between the latent and the sensible heating. This is accomplished by evaluating the mass flux of vapour $\dot{m_{vap}}[kg.m^{-2}.s^{-1}]$ produced on an area A_L(following the cycle defined in Fig.2), and multiplying it by the latent heat of vaporization $L[j/kg]$

$$Q_{vap} = A_L \cdot \dot{m}_{vap} \cdot \Delta H_{vap} \tag{17}$$

Where the evaporation rate is defined according to the work of (Bird et al. (1960)) and (Stull (2017)). The mass flux of water vapor $\dot{m_{vap}}$ is driven by the concentration gradient between the gas and the liquid, in accordance with Fick's law of diffusion for a perfect, stationary gas(Khandekar and Muralidhar (2020)) whose diffusivity is denoted as $D_{L,G}$.

$$\begin{aligned} \dot{m}_{vap}(t) &= -\rho_g \cdot D_{L,g} \cdot \frac{d\omega_L}{dy} \\ &\approx -\rho_g \cdot D_{L,g} \cdot \frac{\omega_{sat}(t) - \omega_{vap,g}(t)}{\delta} \end{aligned} \tag{18}$$

The concentration is established between the saturated interface at a pressure $P_{sat}[Pa]$ and the chamber characterised at the temperature $T_G[K]$, pressure $P_g[Pa]$ and radius $r[mm]$. The mass fraction of vapour at the saturated interface, denoted as ω_{sat}, is given by:

$$\omega_{sat}(t) = \frac{M_g}{M_L} \cdot \frac{P_{sat}(t)}{P_g(t) - P_{sat}(t)} \tag{19}$$

Whereas $\omega_{vap,g}$, the fractional mass of vapour in the chamber can be expressed according to Dalton's law (Stull (2017)):

$$\omega_{vap,g}(t) = \frac{m_{vap}(t)}{m_{air} + m_{vap}(t)} \tag{20}$$

The mass vapour flux $\dot{m}_{vap}$ flows from an in-contact interface over a distance $\delta[m]$ into the surrounding air. This distance is approximated as follows:

$$\delta = \sqrt{D_{L,g} \cdot \Delta t} \tag{21}$$

The process is driven by diffusion under the assumption of steady-state conditions. The mass flux is derived from Fick's Law of Diffusion, which states that the diffusive flux is proportional to the concentration gradient.

Saturation pressure P_{sat} represents the pressure at which evaporation and condensation are in equilibrium for a given temperature, indicating that the air is saturated and cannot accommodate any additional water vapour. It can be derived from *Claudius Clapeyron* equations for a certain temperature T_L:

$$P_{sat}(t) = P_{ref} \cdot e^{-\frac{L}{R_v} \cdot (\frac{1}{T_L(t)} - \frac{1}{T_{ref}})} \tag{22}$$

This empirical relationship approximates the saturation pressure P_{sat} at a temperature $T_L(t)$ based on a pair of values $(T_{ref}[K], P_{ref}[Pa])$ corresponding to the saturated temperature at a given condition.Additionally, $L[J \cdot kg^{-1}]$ represents the latent heat of vaporization and $R_v[J \cdot K^{-1} \cdot kg^{-1}]$ denotes the specific gas constant for water vapour. The initial mass of air in the system is considered constant m_{air}, while the initial vapour rate is set to zero $m_{vap}(t = 0) = 0$.
By applying the Euler discretisation defined in equation 13, we derive from equation (18):

$$m_{vap}(t+\Delta t) = m_{vap}(t) - \sqrt{D_{L,g} \cdot \Delta t} \cdot \rho_g \cdot \Delta\omega \tag{23}$$

With:

$$\Delta\omega = \omega_{sat}(t) - \omega_{vap}(t) \tag{24}$$

2.4 Fluido-Kinetic Phase

Once the evaporation rate is identified, we can calculate the increase in both pressure P_g and radius r of the soft chamber by modelling the deformation under pressure of the chamber.

Pressure Increase Assuming the gas generated is perfect, the pressure in the chamber evolves proportionally to the total amount of gas m_{gas} in the chamber. The volume of this chamber is denoted as $V[mm^3]$:

$$V(t) = \frac{4}{3} \cdot \pi \cdot r(t)^3 \tag{25}$$

And the pressure increase is expressed as:

$$P_g(t) = \underbrace{\frac{3 \cdot R}{4 \cdot \pi \cdot M_L}}_{\lambda_1} \cdot \frac{T_g(t)}{r(t)^3} \cdot m_{gas}(t) \tag{26}$$

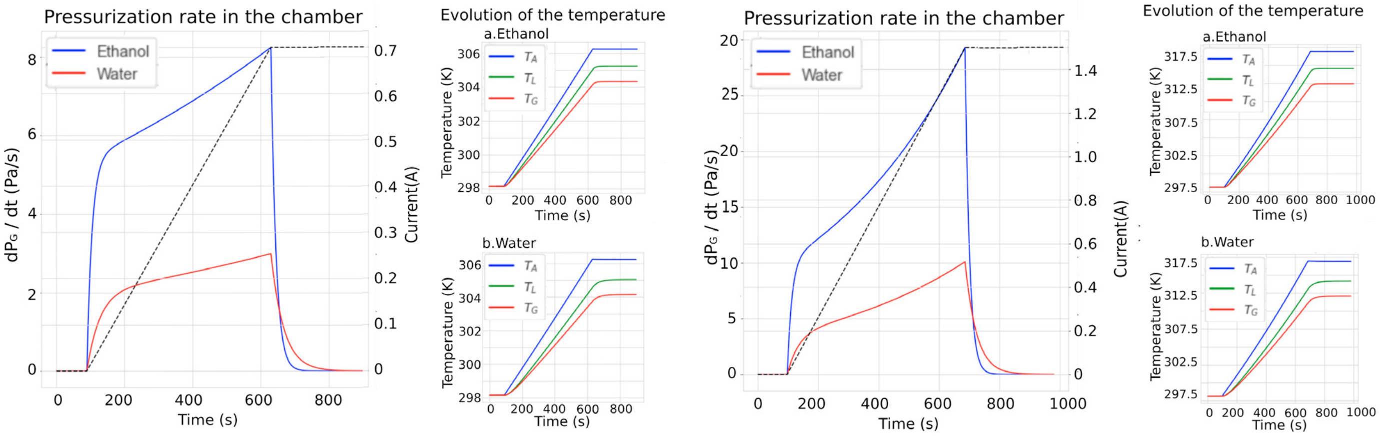

(a) Evolution of the pressure and temperatures over time, for $I_{max} = 0.7[A]$

(b) Evolution of the pressure and temperatures over time, for $I_{max} = 1.5[A]$

Fig. 3. Temporal evolution of system pressurisation and temperature for different maximal input currents (0.7 A and 1.5 A) and working fluids (ethanol and water)

Radius Increase In our case, we are simulating a soft, spherical chamber that will deform under said pressure. Soft materials present hyperelastic behaviours, complicating the simulation of their mechanical response to stress. As simplification we used the Young-Laplace model, described in (Hirai et al. (2021)), which links the strain of a spherical chamber to the difference in pressure between the ambient pressure P_{env} and chamber pressure P_g, via the surface tension of the material $\gamma[N \cdot m^{-1}]$ and its thickness $d_{sh}[mm]$.

$$\begin{aligned} P_g(t) &= \frac{2 \cdot \gamma}{r(t)} + P_{env} \\ &= 2 \cdot \underbrace{E \cdot r(0) \cdot d_{sh}}_{\lambda_2} \cdot \frac{(r(t) - r(0))}{r(t)^3} + P_{env} \end{aligned} \tag{27}$$

By subtracting equations (27) and (26), we isolate and express the radius $r(t)$ as a function of the gas temperature $T_g(t)$ and the total mass of gas in the chamber $m_{gas}(t)$:

$$P_{env} \cdot r(t)^3 + \lambda_2 \cdot r(t) - \lambda_2 \cdot r(0) - \lambda_1 \cdot T_g(t) \cdot m_{gas}(t) = 0 \tag{28}$$

Equation (28) is highly nonlinear, making analytical solutions either impractical or impossible for most parameter sets. Consequently, numerical methods such as the root-finding algorithm implemented in *fsolve* (*numpy*) are required, although they may cause instabilities in the system.

3. RESULTS

3.1 Implementation

The model was implemented in Python using the *numpy* and *matplotlib* libraries for numerical computation and visualisation, respectively.
This study focuses on modelling small actuators for minimally invasive surgery applications, which influenced the selection of dimensions. The actuator's initial radius is defined as $r(t = 0) = 5.5[mm]$, while the reservoir and liquid interfaces are set at $4.5[mm]$. The system is initialised with uniform temperature conditions, such that

$$T_A = T_B = T_L = T_G = T_{env} \tag{29}$$

And equal pressures:

$$P_{env} = P_G[Pa] \tag{30}$$

We selected the Peltier element CP076581-238P ($6.5 \cdot 8.1 \cdot 2.77mm$) which aligns well with the overall design constraints of the system.
We simulated a ramped current, increasing from 0 to 0.7 / 1.5 Amperes over 1000 seconds, incorporating small constant periods before and after the ramp to assess the system's stability. Additionally, we studied the model's response for two liquids—water and ethanol—during the heating process. All associated parameters were considered constant over the temperature and selected at T_{env}.

3.2 Results

The results to the simulation conducted are presented in Fig.3a and Fig.3b. The model's behaviour is interdependent on various variables, making it challenging to isolate the effects of individual parameters. While some variables may exhibit clearer or stronger responses, it is crucial to consider the system as a whole, as the interactions among these elements significantly impact overall behaviour.

We here examined the temporal evolution of the pressurisation rate, P_g, for two current values I and two working fluids: ethanol and water. Ethanol, with a lower boiling point ($351K$ at atmospheric pressure) compared to water, evaporates faster under the same conditions, resulting in a more rapid pressure increase within the chamber for both current values (Fig.3a and Fig.3b). This behaviour highlights the intrinsic relationship between fluid properties and the thermal energy supplied to the system.

As the current stabilises, the system's temperatures and pressurisation rates also reach a steady state, highlighting the direct proportionality between heat flow and pressure generation. Notably, an increase in current leads to a marked rise in system temperature for both fluids, averaging a factor of 2.5. Simultaneously, the maximum pressurisation rate experiences an even more pronounced increase, averaging a threefold enhancement. For example, in the case of ethanol, the maximum pressurisation rate rises from approximately $dP/dt \approx 8.2 Pa/s$ to $dP/dt \approx 28 Pa/s$ as the maximum current is increased.

While the system showed a coherent response, the magnitude of this response was smaller than anticipated: this discrepancy highlights the need for further refinement of the model parameters. This could be attributed to the numerous variables used in our model, which may not be perfectly fitted to our situation. However, with our current model, we demonstrate an evolution of the pressure in the chamber that is both coherent and stable. Although the values obtained do not entirely align with those expected from the state of the art, we believe that further fine-tuning of the parameters will enable us to refine the model, particularly for applications in soft robotics actuation solutions.

4. CONCLUSION

This study presents a comprehensive multi-physics model for evaporation-driven actuation in soft robotics, addressing critical challenges associated with untethered phase-change-based systems. By integrating electrothermal, thermo-fluidic, and mechanical processes, the model aims to provide an innovative framework for analysing and optimising the performance of soft actuators. It proposes a direct relationship between electrical energy input and mechanical work output.

The key strength of the model lies in its ability to couple diverse physical domains. The interaction between heat transfer, liquid evaporation, and material deformation is captured through dynamic feedback mechanisms, offering insights into the fundamental trade-offs governing phase-change actuation. For instance, the iterative simulation of vapour generation, chamber pressure, and actuator deformation highlights the complex interplay of thermodynamics and material mechanics, which is critical for achieving precise control and responsiveness. Furthermore, focusing on the pre-boiling operational regimes explores the potential for reducing thermal gradients, shortening actuation times, and improving system efficiency.

In conclusion, the proposed model not only deepens our understanding of evaporation-driven actuation but also lays the groundwork for future innovations in the field, offering new possibilities for untethered, responsive, and adaptive soft systems.

ACKNOWLEDGEMENTS

We acknowledge the support of the European Union by the Next Generation EU project ECS00000017 'Ecosis tema dell'Innovazione' Tuscany Health Ecosystem (THE, PNRR, Spoke 9: Robotics and Automation for Health)

REFERENCES

Bell, M.A., Gorissen, B., Bertoldi, K., Weaver, J.C., and Wood, R.J. (2022). A modular and self-contained fluidic engine for soft actuators. *Advanced Intelligent Systems*. doi:10.1002/aisy.202100094.

Bird, R.B., Stewart, W.E., and Lightfoot, E.N. (1960). *Transport phenomena*. J. Wiley and sons.

Exley, T., Johnson, D., and Jafari, A. (2023). Utilizing the peltier effect for actuation of thermo-active soft robots. *Smart Materials and Structures*. doi: 10.1088/1361-665X/ace225.

Garrad, M., Feeney, I., Conn, A.T., Rossiter, J., Nemitz, M.P., and Hauser, H. (2021). An all soft, electro-pneumatic controller for soft robots. In *2021 IEEE 4th International Conference on Soft Robotics (RoboSoft)*. IEEE. doi:10.1109/RoboSoft51838.2021.9479381.

Garrad, M., Soter, G., Conn, A.T., Hauser, H., and Rossiter, J. (2019). Driving soft robots with low-boiling point fluids. In *2019 2nd IEEE International Conference on Soft Robotics (RoboSoft)*. doi: 10.1109/ROBOSOFT.2019.8722812.

Han, J., Jiang, W., Niu, D., Li, Y., Zhang, Y., Lei, B., Liu, H., Shi, Y., Chen, B., Yin, L., Liu, X., Peng, D., and Lu, B. (2019). Untethered soft actuators by liquid–vapor phase transition: Remote and programmable actuation. *Advanced Intelligent Systems*. doi:10.1002/aisy.201900109.

Hirai, S., Nagatomo, T., Hiraki, T., Ishizuka, H., Kawahara, Y., and Miki, N. (2021). Micro elastic pouch motors: Elastically deformable and miniaturized soft actuators using liquid-to-gas phase change. *IEEE Robotics and Automation Letters*. doi: 10.1109/LRA.2021.3075102.

Huber, J.E., Fleck, N.A., and Ashby, M.F. (1997-10-08). The selection of mechanical actuators based on performance indices. *Proceedings of the Royal Society of London. Series A: Mathematical, Physical and Engineering Sciences*, 453. doi:10.1098/rspa.1997.0117. Publisher: Royal Society.

Khandekar, S. and Muralidhar, K. (2020). *Drop Dynamics and Dropwise Condensation on Textured Surfaces*. Mechanical Engineering Series. Springer International Publishing. doi:10.1007/978-3-030-48461-3.

Lee, H.J., Prachaseree, P., and Loh, K.J. (2021). Rapid soft material actuation through droplet evaporation. *Soft Robotics*. doi:10.1089/soro.2020.0055.

Li, Y., Ren, T., Chen, Y., Zhou, J., Hu, Y., Wang, Z., Sun, W., and Xiong, C. (2021). Untethered multimode fluidic actuation: A new approach to soft and compliant robotics. *Soft Robotics*. doi:10.1089/soro.2019.0131.

Schmitt, F., Piccin, O., Barbé, L., and Bayle, B. (2018). Soft robots manufacturing: A review. *Frontiers in Robotics and AI*. doi:10.3389/frobt.2018.00084.

Stull, R.B. (2017). *Practical meteorology: an algebra-based survey of atomspheric science*. UBC, v1.02b edition.

Wehner, M., Tolley, M.T., Mengüç, Y., Park, Y.L., Mozeika, A., Ding, Y., Onal, C., Shepherd, R.F., Whitesides, G.M., and Wood, R.J. (2014). Pneumatic energy sources for autonomous and wearable soft robotics. *Soft Robotics*. doi:10.1089/soro.2014.0018.

Wehner, M., Truby, R.L., Fitzgerald, D.J., Mosadegh, B., Whitesides, G.M., Lewis, J.A., and Wood, R.J. (2016). An integrated design and fabrication strategy for entirely soft, autonomous robots. *Nature*. doi: 10.1038/nature19100.

Xu, Y., Wang, T., and Wang, Z. (2021). A soft actuator with integrated pneumatic source using electrically induced liquid-to-gas conversion. In *2021 IEEE International Conference on Robotics and Biomimetics (ROBIO)*. doi:10.1109/ROBIO54168.2021.9739313.